Cite as: L. Traunmüller *et al*., *Science* 10.1126/science.aaf2397 (2016).

Control of neuronal synapse specification by a highly dedicated alternative splicing program

Lisa Traunmüller,* Andrea M. Gomez,* Thi-Minh Nguyen, Peter Scheiffele†

Biozentrum, University of Basel Klingelbergstrasse 50-70, 4056 Basel, Switzerland

*These authors contributed equally to this work.

†Corresponding author. Email: peter.scheiffele@unibas.ch

Alternative RNA splicing represents a central mechanism for expanding the coding power of genomes. Individual RNA-binding proteins can control alternative splicing choices in hundreds of RNA transcripts, thereby tuning amounts and functions of large numbers of cellular proteins. We found that the RNA-binding protein SLM2 is essential for functional specification of glutamatergic synapses in the mouse hippocampus. Genome-wide mapping revealed a markedly selective SLM2-dependent splicing program primarily consisting of only a few target messenger RNAs that encode synaptic proteins. Genetic correction of a single SLM2-dependent target exon in the synaptic recognition molecule neurexin-1 was sufficient to rescue synaptic plasticity and behavioral defects in *Slm2* knockout mice. These findings uncover a highly selective alternative splicing program that specifies synaptic properties in the central nervous system.

Alternative splicing provides a key mechanism for neuron-specific gene expression (*1*–*3*). An array of RNA-binding proteins broadly expressed in neuronal cells has been implicated in controlling developmentally regulated and neuron-specific alternative splicing programs, with single proteins regulating hundreds of target transcripts (*4*–*6*). However, some RNA-binding proteins are selectively expressed in neuronal populations, raising the possibility that they may control cell type– and synapse-specific functions (*7*, *8*).

The KH-domain RNA-binding protein SLM2 is highly expressed in glutamatergic pyramidal cells of the mouse hippocampus and in a specific subset of γ-aminobutyric acid (GABA)–releasing interneurons (*9*, *10*). In $Slm2^{KO}$ knockout (KO) mice, glutamatergic spine synapses formed at normal numbers on the primary apical dendrites of hippocampal CA1 neurons (Fig. 1, A and B). Western blot analysis of synaptosome fractions from wild-type (WT) and $Slm2^{KO}$ hippocampi revealed overall normal concentrations of glutamatergic synapse proteins. However, there was an increase in the AMPA-type glutamate receptor (AMPAR) subunit GluA1, in particular in detergent-soluble fractions from adult $Slm2^{KO}$ mouse synaptosomes (Fig. 1, Cand D). In acute slices from adolescent mice (postnatal day 25), GluA1 amounts were elevated in total cell lysates and cell surface fractions, whereas *N*-methyl-d-aspartate (NMDA)–receptor GluN1 subunit expression was unaltered (Fig. 1, E and F). Whole-cell voltage-clamp recordings from CA1 neurons in $Slm2^{KO}$ hippocampal slices showed no difference in the miniature excitatory postsynaptic current (mEPSC) amplitude and frequency between WT and $Slm2^{KO}$ mice (Fig. 2, A and B). However, mEPSC events showed a modest increase in the speed of rise and decay times in $Slm2^{KO}$ CA1 neurons (Fig. 2, C and D). AMPAR/NMDAR ratios were significantly increased in $Slm2^{KO}$ mice (Fig. 2, E and F). In $Slm2^{KO}$ CA1 neurons, stimulation of Schaffer collaterals elicited larger postsynaptic responses as compared to WT (Fig. 2G; see also fig. S1A for data from field EPSP recordings). Paired-pulse facilitation was normal in $Slm2^{KO}$ (Fig. 2H). In sum, these experiments demonstrate an elevation in postsynaptic AMPAR surface expression and function in CA1 neurons of $Slm2^{KO}$ mice. Finally, long-term potentiation (LTP) induced by theta-burst stimulation of Schaffer collaterals was significantly reduced in acute slices from $Slm2^{KO}$ mice (Fig. 2I).

Candidate gene approaches have identified some transcripts that are altered in $Slm2^{KO}$ brains (*9*–*12*). However, a comprehensive global analysis of SLM2 targets is lacking. Using Illumina paired-end sequencing we mapped SLM2-dependent alternative splicing events at a genome-wide level. This analysis revealed highly correlated expression of transcripts between genotypes, indicating that SLM2 does not play a major role in tuning overall transcript levels (Fig. 3A). Moreover, transcripts encoding ionotropic and metabotropic glutamate receptors were not significantly changed (fig. S1, B to E). Most significantly altered was the transcript encoding the SLM2 paralogue SLM1, which has previously been shown to be up-regulated in $Slm2^{KO}$ hippocampus (*11*).

Genome-wide splicing patterns were extracted on the basis of annotations from FAST DB, and splicing indices calculated. The vast majority of exons remained essentially

unchanged between WT and *Slm2*^{KO} hippocampi (Fig. 3B and fig. S2A; analysis includes 4965 microexons). Notably, alternative exons in four genes showed disproportionately strong deregulation in the *Slm2*^{KO} hippocampus. There was a >2-fold increase in the incorporation of exons at the alternatively spliced segment four (AS4) of neurexins (*Nrxn1*, *2*, and *3*), three genes that encode synaptic cell surface receptors. Moreover, exon 24 incorporation was 1.58-fold elevated in tomosyn-2 (*Stxbp5l*), a component of the vesicle fusion machinery. Another seven exons were identified that exhibited significant alterations ($P < 0.01$) although with modest fold-change (Fig. 3C and table S1). Independent experimental validation confirmed that deregulation of additional candidate target exons was small or in some cases not detectable (Fig. 3, D and E, and fig. S2B). The paralogue SLM1 may compensate for the loss of SLM2 (*11*). However, comparison of candidate exons in *Slm1*^{KO}, *Slm2*^{KO}, and *Slm1:Slm2*^{DKO} (double knockout) mice revealed that deregulation was not significantly more severe in the DKO mice (fig. S2C).

Alternative splicing at *Nrxn* AS4 regulates selective trans-synaptic interactions of neurexins in the presynaptic terminal with several synaptic receptors (*13*–*16*). For an unbiased identification of interaction partners regulated by this alternative splicing event, we performed affinity purifications on recombinant NRX1β4(+) and NRX1β4(-) isoforms, followed by shot-gun mass spectrometry (Fig. 4A and fig. S3, A and B). We identified 21 candidate binding partners, including known neurexin-binding proteins (Cbln2, the leucine-rich repeat proteins LRRTM1,2,4, neuroligin-1,2, 3, and the sortilin-related VPS10-domain containing receptor SORCS) and a number of previously unknown candidate ligands (complement C3, chondroadherin-like protein, neuronal pentraxin and neuronal pentraxin receptor 1, and astrotactin). For six of these proteins, we observed significant differences in the interaction with AS4(+) and AS4(-) NRX1β isoforms, including neuroligins, Chadl, LRRTMs, and complement C3 (Fig. 4B and table S2; $P < 0.05$). Thus, there is an array of synaptic interactions that can be modified by deregulation of neurexin alternative splicing in *Slm2*^{KO} mice.

We hypothesized that the modification of endogenous neurexin alternative splicing in *Slm2*^{KO} hippocampus may disrupt interactions with these splice insertion-sensitive ligands. In coimmunoprecipitation experiments with an antibody against neurexin-1 (anti-neurexin-1), we observed that neuroligin-1 (NL1) and neuroligin-3 (NL3) are abundant in immunoprecipitates from WT mice. However, both NLs were reduced in precipitates prepared from *Slm2*^{KO} mice (Fig. 4C). Conversely, coprecipitation of C3, a component of the complement system that has been implicated in synapse elimination (*17*), was slightly elevated in the same precipitates from *Slm2*^{KO} mice (fig. S3C). Thus, the loss of SLM2 indeed switches synaptic receptor-ligand interactions. NL1 recruits synaptic NMDA receptors (*18*, *19*), whereas NL3 and LRRTMs mediate the synaptic recruitment and stabilization of AMPA receptors (*20*). Loss of the trans-synaptic interactions with these neurexin ligands might result in the postsynaptic glutamate receptor deficits in *Slm2*^{KO} mice. To test this hypothesis, we generated *Nrxn1*$^{\Delta ex21}$ mice in which *Nrxn1* exon 21 (the alternative cassette exon at AS4) is specifically deleted but total *Nrxn* transcript levels are unchanged (fig. S4, A to C). Heterozygous removal of one *Nrxn1*$^{\Delta ex21}$ allele restored normal *Nrxn1* AS4(-) transcript levels in the *Slm2*^{KO} background (Fig. 4D). Restoration of *Nrxn1* AS4(-) transcripts rescued trans-synaptic cell surface interactions of endogenous neurexin with NL1 and NL3 in the coimmunoprecipitation assays (Fig. 4E), normalized GluA1 amounts in acute hippocampal slices (Fig. 4F), and partially recovered theta burst–induced Schaffer collateral LTP (Fig. 4G). In an object recognition test, a behavioral task that involves the hippocampus (*21*), *Slm2*^{KO} mice differed significantly from WT mice in that they did not preferentially explore novel objects (Fig. 4, H and I, and fig. S4D). Also, this phenotype and other behavioral alterations were rescued in *Slm2*^{KO}*;Nrxn1*$^{\Delta ex21/+}$ mice (Fig. 4, H and I, and fig. S4, E to G). Thus, the control of a single alternative exon by SLM2 has a major contribution to the specification of glutamatergic synapse function, plasticity, and mouse behavior.

Forced expression of *Nrxn3* AS4(+) isoforms was previously shown to reduce postsynaptic AMPAR localization and to impair LTP in the subiculum (*22*). By contrast, in *Slm2*^{KO} CA1 neurons, total surface AMPAR amounts and AMPAR function are elevated. These differences are most likely due to the simultaneous disruption of alternative splicing in all three neurexin genes in the *Slm2*^{KO}, as well as the different cell type–specific context. Compared to other RNA-binding proteins, SLM2 exhibits highly selective neuronal cell type–specific expression, and only a small set of alternative exons is particularly reliant on SLM2 function. Our genetic rescue experiments demonstrate that restoration of a single alternative exon has a major impact on the *SLM2*^{KO} phenotype. We hypothesize that targeted, cell type–specific splicing regulation of surface receptor recognition systems as reported here for the SLM2-neurexin system represents a general mechanism for the control of synapse specification in neuronal circuits.

REFERENCES AND NOTES

1. S. Zheng, D. L. Black, Alternative pre-mRNA splicing in neurons: Growing up and extending its reach. *Trends Genet.* **29**, 442–448 (2013). doi:10.1016/j.tig.2013.04.003 Medline
2. B. Raj, B. J. Blencowe, Alternative splicing in the mammalian nervous system: Recent insights into mechanisms and functional roles. *Neuron* **87**, 14–27 (2015). doi:10.1016/j.neuron.2015.05.004 Medline

3. D. Schreiner, T.-M. Nguyen, G. Russo, S. Heber, A. Patrignani, E. Ahrné, P. Scheiffele, Targeted combinatorial alternative splicing generates brain region-specific repertoires of neurexins. *Neuron* **84**, 386–398 (2014).doi:10.1016/j.neuron.2014.09.011 Medline
4. J. Ule, A. Ule, J. Spencer, A. Williams, J.-S. Hu, M. Cline, H. Wang, T. Clark, C. Fraser, M. Ruggiu, B. R. Zeeberg, D. Kane, J. N. Weinstein, J. Blume, R. B. Darnell, Nova regulates brain-specific splicing to shape the synapse. *Nat. Genet.* **37**, 844–852 (2005).doi:10.1038/ng1610 Medline
5. M. Quesnel-Vallières, M. Irimia, S. P. Cordes, B. J. Blencowe, Essential roles for the splicing regulator nSR100/SRRM4 during nervous system development. *Genes Dev.* **29**, 746–759 (2015).doi:10.1101/gad.256115.114 Medline
6. Q. Li, S. Zheng, A. Han, C. H. Lin, P. Stoilov, X. D. Fu, D. L. Black, The splicing regulator PTBP2 controls a program of embryonic splicing required for neuronal maturation. *eLife* **3**, e01201 (2014). Medline
7. D. Schreiner, T. M. Nguyen, P. Scheiffele, Polymorphic receptors: Neuronal functions and molecular mechanisms of diversification. *Curr. Opin. Neurobiol.* **27**, 25–30 (2014).doi:10.1016/j.conb.2014.02.009 Medline
8. A. D. Norris, S. Gao, M. L. Norris, D. Ray, A. K. Ramani, A. G. Fraser, Q. Morris, T. R. Hughes, M. Zhen, J. A. Calarco, A pair of RNA-binding proteins controls networks of splicing events contributing to specialization of neural cell types. *Mol. Cell* **54**, 946–959 (2014).doi:10.1016/j.molcel.2014.05.004 Medline
9. I. Ehrmann, C. Dalgliesh, Y. Liu, M. Danilenko, M. Crosier, L. Overman, H. M. Arthur, S. Lindsay, G. J. Clowry, J. P. Venables, P. Fort, D. J. Elliott, The tissue-specific RNA binding protein T-STAR controls regional splicing patterns of neurexin pre-mRNAs in the brain. *PLOS Genet.* **9**, e1003474 (2013).doi:10.1371/journal.pgen.1003474 Medline
10. T. Iijima, Y. Iijima, H. Witte, P. Scheiffele, Neuronal cell type-specific alternative splicing is regulated by the KH domain protein SLM1. *JCB* **204**, 331–342 (2014).doi:10.1083/jcb.201310136 Medline
11. L. Traunmüller, C. Bornmann, P. Scheiffele, Alternative splicing coupled nonsense-mediated decay generates neuronal cell type-specific expression of SLM proteins. *J. Neurosci.* **34**, 16755–16761 (2014).doi:10.1523/JNEUROSCI.3395-14.2014 Medline
12. T. Iijima, K. Wu, H. Witte, Y. Hanno-Iijima, T. Glatter, S. Richard, P. Scheiffele, SAM68 regulates neuronal activity-dependent alternative splicing of neurexin-1. *Cell* **147**, 1601–1614 (2011).doi:10.1016/j.cell.2011.11.028 Medline
13. A. A. Boucard, A. A. Chubykin, D. Comoletti, P. Taylor, T. C. Südhof, A splice code for trans-synaptic cell adhesion mediated by binding of neuroligin 1 to α- and β-neurexins. *Neuron* **48**, 229–236 (2005).doi:10.1016/j.neuron.2005.08.026 Medline
14. B. Chih, L. Gollan, P. Scheiffele, Alternative splicing controls selective trans-synaptic interactions of the neuroligin-neurexin complex. *Neuron* **51**, 171–178 (2006).doi:10.1016/j.neuron.2006.06.005 Medline
15. T. Uemura, S.-J. Lee, M. Yasumura, T. Takeuchi, T. Yoshida, M. Ra, R. Taguchi, K. Sakimura, M. Mishina, Trans-synaptic interaction of GluRdelta2 and Neurexin through Cbln1 mediates synapse formation in the cerebellum. *Cell* **141**, 1068–1079 (2010).doi:10.1016/j.cell.2010.04.035 Medline
16. K. Matsuda, M. Yuzaki, Cbln family proteins promote synapse formation by regulating distinct neurexin signaling pathways in various brain regions. *Eur. J. Neurosci.* **33**, 1447–1461 (2011).doi:10.1111/j.1460-9568.2011.07638.x Medline
17. B. Stevens, N. J. Allen, L. E. Vazquez, G. R. Howell, K. S. Christopherson, N. Nouri, K. D. Micheva, A. K. Mehalow, A. D. Huberman, B. Stafford, A. Sher, A. M. Litke, J. D. Lambris, S. J. Smith, S. W. M. John, B. A. Barres, The classical complement cascade mediates CNS synapse elimination. *Cell* **131**, 1164–1178 (2007).doi:10.1016/j.cell.2007.10.036 Medline
18. B. Chih, H. Engelman, P. Scheiffele, Control of excitatory and inhibitory synapse formation by neuroligins. *Science* **307**, 1324–1328 (2005).doi:10.1126/science.1107470 Medline
19. E. C. Budreck, O.-B. Kwon, J. H. Jung, S. Baudouin, A. Thommen, H.-S. Kim, Y. Fukazawa, H. Harada, K. Tabuchi, R. Shigemoto, P. Scheiffele, J.-H. Kim, Neuroligin-1 controls synaptic abundance of NMDA-type glutamate receptors through extracellular coupling. *Proc. Natl. Acad. Sci. U.S.A.* **110**, 725–730 (2013).doi:10.1073/pnas.1214718110 Medline
20. S. L. Shipman, E. Schnell, T. Hirai, B.-S. Chen, K. W. Roche, R. A. Nicoll, Functional dependence of neuroligin on a new non-PDZ intracellular domain. *Nat. Neurosci.* **14**, 718–726 (2011).doi:10.1038/nn.2825 Medline
21. S. J. Cohen, R. W. Stackman Jr., Assessing rodent hippocampal involvement in the novel object recognition task. A review. *Behav. Brain Res.* **285**, 105–117 (2015).doi:10.1016/j.bbr.2014.08.002 Medline
22. J. Aoto, D. C. Martinelli, R. C. Malenka, K. Tabuchi, T. C. Südhof, Presynaptic neurexin-3 alternative splicing trans-synaptically controls postsynaptic AMPA receptor trafficking. *Cell* **154**, 75–88 (2013).doi:10.1016/j.cell.2013.05.060 Medline
23. G. Feng, R. H. Mellor, M. Bernstein, C. Keller-Peck, Q. T. Nguyen, M. Wallace, J. M. Nerbonne, J. W. Lichtman, J. R. Sanes, Imaging neuronal subsets in transgenic mice expressing multiple spectral variants of GFP. *Neuron* **28**, 41–51 (2000).doi:10.1016/S0896-6273(00)00084-2 Medline
24. E. C. Budreck, P. Scheiffele, Neuroligin-3 is a neuronal adhesion protein at GABAergic and glutamatergic synapses. *Eur. J. Neurosci.* **26**, 1738–1748 (2007).doi:10.1111/j.1460-9568.2007.05842.x Medline
25. K. Muhammad, S. Reddy-Alla, J. H. Driller, D. Schreiner, U. Rey, M. A. Böhme, C. Hollmann, N. Ramesh, H. Depner, J. Lützkendorf, T. Matkovic, T. Götz, D. D. Bergeron, J. Schmoranzer, F. Goettfert, M. Holt, M. C. Wahl, S. W. Hell, P. Scheiffele, A. M. Walter, B. Loll, S. J. Sigrist, Presynaptic spinophilin tunes neurexin signalling to control active zone architecture and function. *Nat. Commun.* **6**, 8362 (2015).doi:10.1038/ncomms9362 Medline
26. G. R. Phillips, J. K. Huang, Y. Wang, H. Tanaka, L. Shapiro, W. Zhang, W.-S. Shan, K. Arndt, M. Frank, R. E. Gordon, M. A. Gawinowicz, Y. Zhao, D. R. Colman, The presynaptic particle web: Ultrastructure, composition, dissolution, and reconstitution. *Neuron* **32**, 63–77 (2001).doi:10.1016/S0896-6273(01)00450-0 Medline
27. D. Schreiner, J. Simicevic, E. Ahrné, A. Schmidt, P. Scheiffele, Quantitative isoform-profiling of highly diversified recognition molecules. *eLife* **4**, e07794 (2015).doi:10.7554/eLife.07794 Medline
28. T. Glatter, C. Ludwig, E. Ahrné, R. Aebersold, A. J. R. Heck, A. Schmidt, Large-scale quantitative assessment of different in-solution protein digestion protocols reveals superior cleavage efficiency of tandem Lys-C/trypsin proteolysis over trypsin digestion. *J. Proteome Res.* **11**, 5145–5156 (2012).doi:10.1021/pr300273g Medline
29. A. Dobin, C. A. Davis, F. Schlesinger, J. Drenkow, C. Zaleski, S. Jha, P. Batut, M. Chaisson, T. R. Gingeras, STAR: Ultrafast universal RNA-seq aligner. *Bioinformatics* **29**, 15–21 (2013).doi:10.1093/bioinformatics/bts635 Medline
30. L. Noli, A. Capalbo, C. Ogilvie, Y. Khalaf, D. Ilic, Discordant Growth of Monozygotic twins starts at the blastocyst stage: A case study. *Stem Cell Reports* **5**, 946–953 (2015).doi:10.1016/j.stemcr.2015.10.006 Medline
31. S. Gandoura, E. Weiss, P.-E. Rautou, M. Fasseu, T. Gustot, F. Lemoine, M. Hurtado-Nedelec, C. Hego, N. Vadrot, L. Elkrief, P. Lettéron, Z. Tellier, M.-A. Pocidalo, D. Valla, D. Lebrec, A. Groyer, R. C. Monteiro, P. de la Grange, R. Moreau, Gene- and exon-expression profiling reveals an extensive LPS-induced response in immune cells in patients with cirrhosis. *J. Hepatol.* **58**, 936–948 (2013).doi:10.1016/j.jhep.2012.12.025 Medline
32. E. Wang, V. Aslanzadeh, F. Papa, H. Zhu, P. de la Grange, F. Cambi, Global profiling of alternative splicing events and gene expression regulated by hnRNPH/F. *PLOS ONE* **7**, e51266 (2012).doi:10.1371/journal.pone.0051266 Medline

ACKNOWLEDGMENTS

We thank O. Mauger, D. Schreiner, and L. Xiao for insightful comments on the manuscript and Y. Hayashi and J. Bischofberger for expert advice. We thank C. Bornmann and P. Demougin, F. Lemoine, P. de la Grange, A. Schmidt, and M. Rüegg for suggestions and experimental support. L.T. was financially supported by the Boehringer Ingelheim Fonds. A.M.G. was supported by a European Molecular Biology Organization long-term fellowship. T.-M.N. was supported by the International PhD Program University of Basel. This work was supported by funds to P.S. from the Swiss National Science Foundation; European Autism Interventions (EU-AIMS, which receives support from the Innovative Medicines Initiative; and the Kanton Basel-Stadt. Sequencing data were deposited at the functional genomics data repository Gene Expression Omnibus (accession number GSE79902).

SUPPLEMENTARY MATERIALS
www.sciencemag.org/cgi/content/full/science.aaf2397/DC1
Materials and Methods
Figs. S1 to S4
Table S1
References (*23*–*32*)

12 January 2016; accepted 15 April 2016
Published online 12 May 2016
10.1126/science.aaf2397

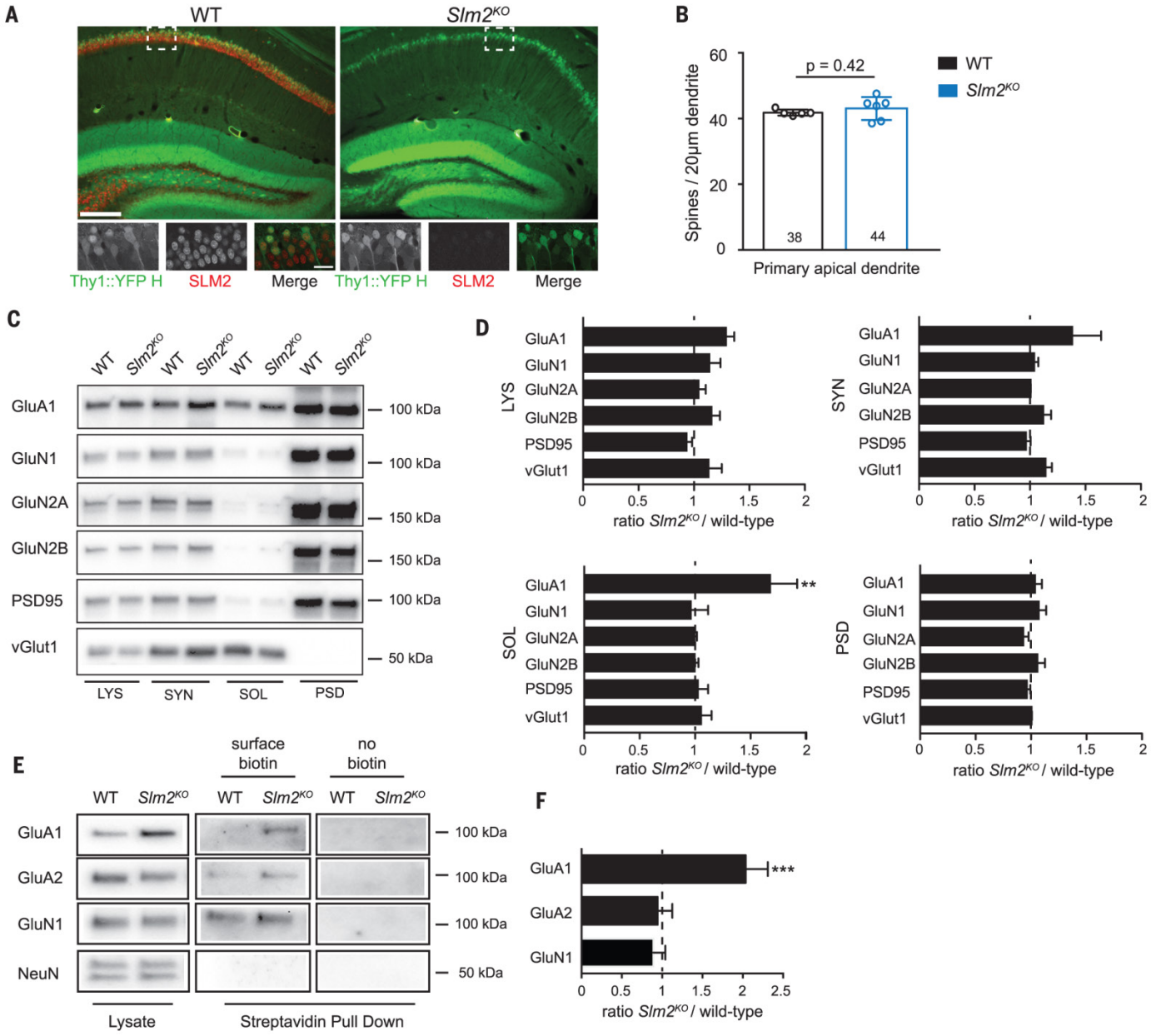

Fig. 1. Synaptic structure and synaptic composition in *Slm2*^{KO} mice. (**A**) Thy1::YFP-H and Thy1::YFP-H:*Slm2*^{KO} hippocampi [yellow fluorescent protein (YFP) in green, anti-SLM2 in red; scale bar, 200 µm (upper panels); 25 µm (lower panels). (**B**) Dendritic spine densities along the primary apical dendrite of CA1 cells in the stratum radiatum (100 µm from pyramidal cell layer). WT: $n = 5$ mice (38 dendrites); *Slm2*^{KO}: $n = 6$ mice (44 dendrites); unpaired t test. (**C**) Western blot analysis of glutamatergic proteins in total lysate (LYS), synaptosomes (SYN), Triton X100–soluble fraction at pH = 6 (SOL), and Triton X100–insoluble postsynaptic density (PSD) in hippocampal tissue from adult WT and *Slm2*^{KO} mice. (**D**) Mean intensities of expression levels in WT and *Slm2*^{KO} hippocampi ($n \geq 3$ mice per genotype, One-way analysis of variance (ANOVA) with Dunnett's multiple comparison test, $^{**}P < 0.01$). (**E**) Total and surface glutamate receptor pools were assessed in acute slices from P25 mice by surface biotinylation and streptavidin pull-down assay; nonbiotinylated samples ("no biotin") served as negative control. (**F**) Quantification for Fig. 1E (one-way ANOVA with Tukey's post-hoc test, $^{***}P < 0.001$, $n \geq 4$ for WT and *Slm2*^{KO}).

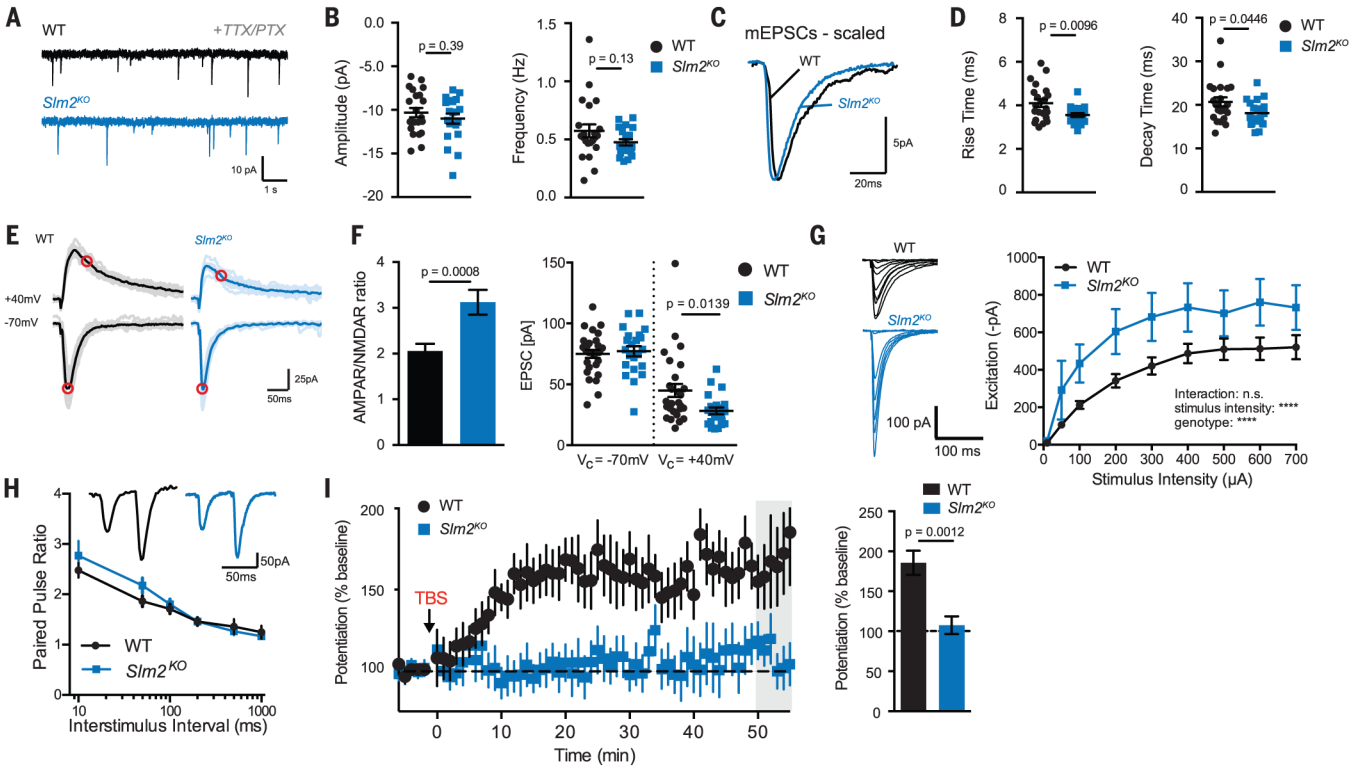

Fig. 2. SLM2 is required for normal glutamatergic transmission and plasticity. (**A** and **B**) Amplitude and frequency of spontaneous mEPSCs recorded from CA1 pyramidal neurons in acute hippocampal slices ($n \geq 20$ per genotype, $n \geq 3$ animals per genotype, mean and SEM, unpaired t test). (**C** and **D**) Average traces of mEPSCs from (A) and (B) scaled to peak amplitude. (**E** and **F**) Average traces and summary data of evoked EPSCs at −70 mV (lower trace) and +40 mV (upper trace), respectively. Peak EPSC amplitudes were measured at −70 mV (peak marked by red circle). NMDAR currents were measured at +40 mV (red circle, $n \geq 22$ per genotype, $n \geq 4$ animals; mean and SEM, unpaired t test). (**G**) Representative traces of EPSCs evoked with varied stimulation intensities in WT or *Slm2*^{KO} CA1 neurons ($n \geq 8$ per genotype, $n \geq 3$ animals; mean and SEM, two-way ANOVA). (**H**) Paired-pulse ratio in CA1 neurons from acute hippocampal slices ($n \geq 11$ per genotype, $n \geq 4$ animals, mean and SEM, two-way ANOVA). (**I**) Averaged responses from *Slm2*^{KO} CA1 neurons following a TBS (theta-burst stimulus) delivered at V_c= −70 mV. The gray bar indicates the interval quantified in the histogram ($n \geq 7$ per genotype, $n \geq 6$ animals, mean and SEM, unpaired t test).

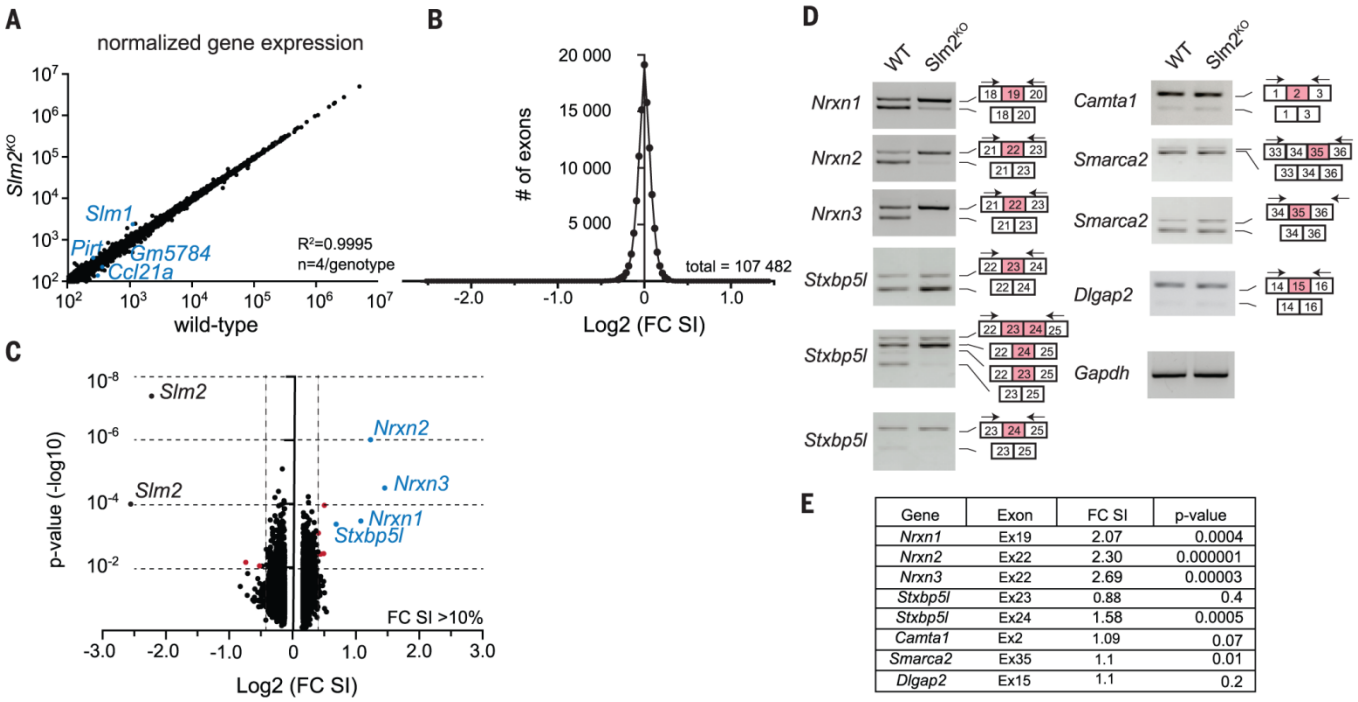

Gene	Exon	FC SI	p-value
Nrxn1	Ex19	2.07	0.0004
Nrxn2	Ex22	2.30	0.000001
Nrxn3	Ex22	2.69	0.00003
Stxbp5l	Ex23	0.88	0.4
Stxbp5l	Ex24	1.58	0.0005
Camta1	Ex2	1.09	0.07
Smarca2	Ex35	1.1	0.01
Dlgap2	Ex15	1.1	0.2

Fig. 3. Genome-wide mapping of SLM2-dependent alternative splicing program. (**A**) Correlation analysis of $\log_{10}$-transformed, normalized total transcript counts (for all genes with count ≥ 100 in *Slm2*^{KO}). Transcripts with significant alteration between genotypes ($P < 0.01$, ΔFC > 50%) are highlighted in blue (n = 4 mice per genotype). (**B**) Frequency distribution of exon incorporation rates for 107,482 exons expressed as fold change in splicing index (FC SI) plotted on a $\log_2$ scale. (**C**) Fold change SI and P-values for all exons with an FC SI > 10% (total of 9110 exons). Exons exhibiting changes of FC SI > 30% and $P <$ 0.01 are marked in red (*Pecam1*, *Epha5*, *Dgkb*, *Gm1673*, *Cpne5*, *Hnrnpul1*, and *Cdk16*; threshold indicated by dashed lines). Highly deregulated exons (FC SI > 50% and $P < 0.01$) are marked in blue (*Nrxn1*, *Nrxn2*, *Nrxn3*, *Stxbp5l*). *Slm2* exon 2, deleted in *Slm2*^{KO}, is not displayed. (**D**) Experimental assessment of candidate SLM2-dependent exons by reverse transcription–polymerase chain reaction (RT-PCR) in WT and *Slm2*^{KO} hippocampi; alternative exons (red), primer sites (arrows). (**E**) Table for fold change SI and P-values for validated exons shown in (D)..

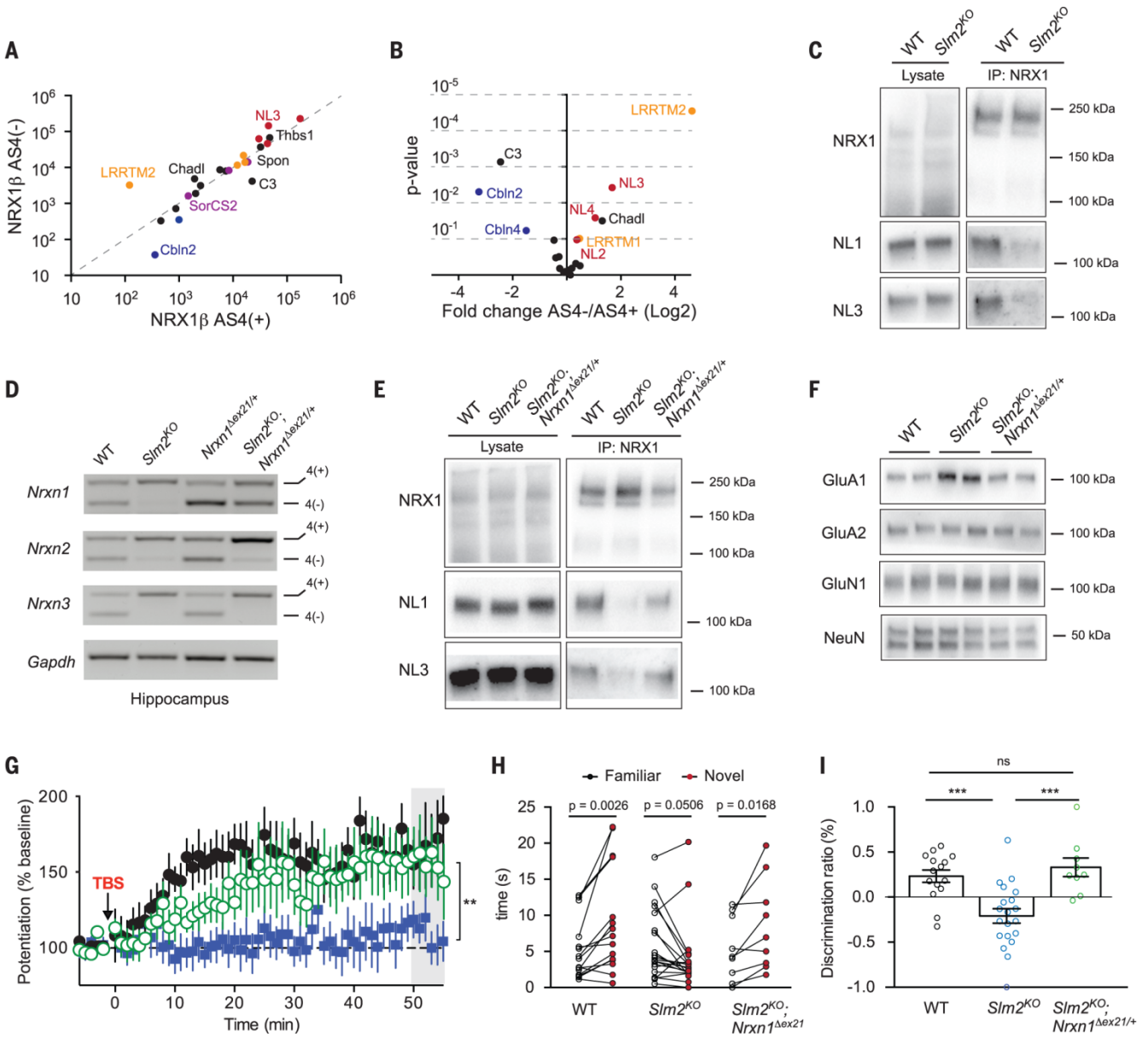

Fig. 4. Heterozygous deletion of *Nrxn1* exon 21 restores synaptic phenotypes in *Slm2*^{KO} hippocampus. (**A**) Affinity purification with recombinant NRX1β AS4(+) and NRX1β AS4(-). Correlation of $\log_{10}$-transformed median spectra counts for all extracellular proteins identified with ≥2 peptides recovered on at least one of the two neurexin isoforms. Paralogues highlighted: NLs (red), Cblns (blue), LRRTMs (orange), SORCs (purple). (**B**) Fold change against *P*-value for all bound extracellular proteins when comparing NRX1β AS4(+) to NRX1β AS4(-). (**C**) Anti-NRX1 immunoprecipitation from forebrain lysates of WT and *Slm2*^{KO} animals probed with anti-NRX1, anti-NL1, and anti-NL3. (**D**) Representative RT-PCR for analysis of *Nrxn1,2,3* AS4 in the hippocampus of WT, *Slm2*^{KO}, *Nrxn*$^{\Delta ex21/+}$ and *Slm2*^{KO};*Nrxn1*$^{\Delta ex21/+}$ animals. (**E**) NRX1 immunoprecipitation from forebrain lysates of WT, *Slm2*^{KO}, and *Slm2*^{KO};*Nrxn1*$^{\Delta ex21/+}$ animals probed with anti-NRX1, anti-NL1 and anti-NL3. (**F**) Glutamate receptor expression in acute slices from P25 WT and *Slm2*^{KO} and *Slm2*^{KO};*Nrxn1*$^{\Delta ex21/+}$ hippocampi. Protein concentrations were probed by Western blotting of total lysates (average FC *Slm2*^{KO}/WT = 1.94, $n = 5$, average FC *Slm2*^{KO};*Nrxn1*$^{\Delta ex21/+}$/WT = 1.13, $n = 3$). (**G**) Averaged responses to a theta-burst stimulation (TBS) in *Slm2*^{KO};*Nrxn1*$^{\Delta ex21/+}$ CA1 neurons (green) is overlaid on WT (gray) and *Slm2*^{KO} responses (blue) from Fig. 2I (n = 8 cells, $n \geq 5$ animals per genotype). Comparison of the responses at 40 to 60 mins after induction between *Slm2*^{KO} and *Slm2*^{KO};*Nrxn1*$^{\Delta ex21+/-}$ by ANOVA with Tukey's multiple comparison test (**$P < 0.01$). (**H** and **I**) Behavioral alterations of WT, *Slm2*^{KO}, and *Slm2*^{KO};*Nrxn1*$^{\Delta ex21}$ mice in object recognition task. Time spent investigating a novel and a familiar object during a 5-min trial 1 hour after acquisition and discrimination ratio are plotted [(H) paired *t* test; (I) unpaired *t* test; WT, $n = 15$; *Slm2*^{KO}, $n = 20$; *Slm2*^{KO};*Nrxn1*$^{\Delta ex21}$, $n = 9$, ns $P > 0.05$; ***$P < 0.001$].

Control of neuronal synapse specification by a highly dedicated alternative splicing program

Lisa Traunmüller, Andrea M. Gomez, Thi-Minh Nguyen and Peter Scheiffele (May 12, 2016)

published online May 12, 2016

Editor's Summary

Science (print ISSN 0036-8075; online ISSN 1095-9203) is published weekly, except the last week in December, by the American Association for the Advancement of Science, 1200 New York Avenue NW, Washington, DC 20005.